

Article

Wavelet Analysis of Ozone Driving Factors Based on ~20 Years of Ozonesonde Measurements in Beijing

Yunshu Zeng¹, Jinqiang Zhang^{2,3,*}, Yajuan Li^{2,4}, Sichang Liu⁵ and Hongbin Chen²

¹ College of Atmospheric Physics, Nanjing University of Information Science and Technology, Nanjing 210044, China; 202311050004@nuist.edu.cn

² Key Laboratory of Middle Atmosphere and Global Environment Observation, Institute of Atmospheric Physics, Chinese Academy of Sciences, Beijing 100029, China; yajuanli@njxzc.edu.cn (Y.L.); chb@mail.iap.ac.cn (H.C.)

³ College of Earth and Planetary Sciences, University of Chinese Academy of Sciences, Beijing 100049, China

⁴ School of Electronic Engineering, Nanjing Xiaozhuang University, Nanjing 211171, China

⁵ Climate Center of Sichuan Province, Chengdu 610072, China; liusichang@mail.iap.ac.cn

* Correspondence: zjq@mail.iap.ac.cn

Abstract: A long-term vertical ozone observational dataset has been provided during 2001–2019 by ozonesonde measurements in Beijing on the North China Plain. Previous studies using this dataset primarily focused on the vertical characteristics of climatological ozone and its variation; however, the driving factors of ozone variation have not been well discussed. In this study, by applying the wavelet analysis method (including continuous wavelet transform and cross wavelet) and sliding correlation coefficients to ~20 years of ozonesonde measurements collected in Beijing, we analyzed the dominant modes of ozone column variability within three height ranges over Beijing (total column ozone: TOT; stratospheric column ozone: SCO; and tropospheric column ozone: TCO). Moreover, we also preliminarily discussed the relationship between these three ozone columns and the El Niño Southern Oscillation (ENSO), Quasi-biennial Oscillation (QBO), and 11-year solar activity cycle. The results revealed that the ozone columns within the three height ranges predominantly adhered to interannual variability patterns, and the short-term variabilities in TOT and SCO may have been related to eruptive volcanic activity. In comparison to the TOT and SCO, the TCO was more susceptible to the forcing influences of high-frequency factors such as pollutant transport. Similar to the results in other mid-latitude regions, strong ENSO and QBO signals were revealed in the interannual ozone column variability over Beijing. The TOT and SCO showed positive anomalous responses to ENSO warm-phase events, and the peak of the ENSO warm phase led the winter peaks of the TOT and SCO by approximately 3–6 months. During the strong cold–warm transition phase in 2009–2012, the TOT and SCO showed a significant positive correlation with the ENSO index. The strong seasonality of the meridional circulation process driven by the QBO led to a significant positive correlation between the QBO index and the TOT and SCO in the interannual cycle, except for two periods of abnormal QBO fluctuations in 2010–2012 and 2015–2017, whereas the TCO showed a time-lagged correlation of approximately 3 months in the annual cycle relative to the QBO due to the influence of the thermodynamic tropopause. In addition, analysis of the F10.7 index and the ozone columns revealed that the ozone columns over Beijing exhibited lagged responses to the peaks of sunspot activity, and there was no obvious correlation between ozone columns and 11-year solar activity cycle. Given the complex driving mechanism of the climatic factors on local ozone variability, the preliminary results obtained in this study still require further validation using longer time series of observational data and the combination of chemical models and more auxiliary data.



Citation: Zeng, Y.; Zhang, J.; Li, Y.; Liu, S.; Chen, H. Wavelet Analysis of Ozone Driving Factors Based on ~20 Years of Ozonesonde Measurements in Beijing. *Atmosphere* **2023**, *14*, 1733. <https://doi.org/10.3390/atmos14121733>

Academic Editors: Haoran Liu, Wei Tan and Wenjing Su

Received: 7 October 2023

Revised: 17 November 2023

Accepted: 22 November 2023

Published: 25 November 2023



Copyright: © 2023 by the authors. Licensee MDPI, Basel, Switzerland. This article is an open access article distributed under the terms and conditions of the Creative Commons Attribution (CC BY) license (<https://creativecommons.org/licenses/by/4.0/>).

Keywords: ozonesonde measurements; ozone columns; wavelet analysis; ozone driving factors

1. Introduction

Atmospheric ozone is a crucial atmospheric component, approximately 90% of which resides within 15–35 km of the stratosphere, and the other 10% of which is distributed within the troposphere. Ozone in the stratosphere plays an important role in absorbing solar ultraviolet radiation, safeguarding human health and maintaining the Earth's ecological balance [1]. High concentrations of tropospheric ozone serve as air pollutants and have significant implications for human health and crop growth [2]. The dynamic variations in ozone concentration are closely associated with geographic locations (latitude and altitude) and seasons. Stratospheric ozone, whose variations are primarily driven by interannual or large-time scale climatic factors [3,4], is mainly formed in the tropics and subsequently transported to the subtropics and high latitudes through atmospheric circulation patterns such as the Brewer–Dobson circulation (BDC) [5]. The production of tropospheric ozone is generally determined by a complex combination of atmospheric dynamics and photochemical reactions. Tropospheric ozone, which is the third most prominent greenhouse gas (next to CO₂ and CH₄) that contributes to climate warming, is primarily generated by a local photochemical reaction of volatile organic compounds (VOCs) and nitric oxide (NO_x); the simple photochemical reaction equation is as follows:



in addition, tropospheric ozone is also affected by short-term weather processes such as stratosphere–troposphere exchange, biomass burning, and pollutant transport [6,7].

Previous studies have extensively employed long-term ozone datasets from local regions (ground-based or satellite measurements) to investigate the dynamic characteristics of stratospheric ozone, tropospheric ozone, and total ozone, as well as the cause of the variation in atmospheric ozone concentration. For instance, by utilizing the total column ozone (TOT) measurements from Dobson at 17 stations within 30° N–60° N during 1961–1990, Krzyścin et al. [8] indicated a strong coupling between TOT in the northern temperate zone and the Quasi-Biennial Oscillation (QBO), El Niño Southern Oscillation (ENSO), and 11-year solar activity cycle; the ozone concentration exhibited substantial reductions during the period of high solar activity and during the periods coinciding with the ENSO warm phase and westerly QBO phase. By applying statistical trend analysis and multivariate linear regression to the ozone dataset from the space-borne Solar Backscatter Ultraviolet Radiometer, Chehade et al. [9] investigated the effects of atmospheric chemical and dynamic factors, including the ENSO, QBO, volcanic activity, 11-year solar activity cycle, and Arctic/Antarctic oscillation, on the long-term change in total ozone. The results highlighted the dominant role of the QBO in tropical ozone variability (± 7 DU), whereas the contribution of volcanic aerosols and ENSO signals to total ozone variability was more pronounced in the northern hemisphere; the solar activity cycle influenced ozone variations across all latitudes. The QBO analyzed in the above studies is a downward-propagating zonal wind variation in the lower tropical stratosphere, with a mean period of approximately 28 months, whose effects are not limited to atmospheric dynamics but also have an impact on chemical constituents such as ozone, vapor, and methane [10]. The QBO couples with ozone variation through complex dynamical and chemical processes, of which dynamical circulation processes are the main driving forces [11]; in particular, the anomalous BDC associated with the QBO can affect the QBO signal from lower latitudes toward the middle and even high latitudes [12]. Regarding the ENSO, it has been suggested that the ENSO is one of the main factors that control the interannual variability of stratospheric ozone [13,14] and that the TOT increases in mid-latitudes during El Niño events [15]. In addition to the QBO and ENSO, volcanic eruptions, the Arctic Oscillation, and the 11-year solar activity cycle are also important driving factors of long-term ozone variation [13,16–19].

The wavelet analysis method, which is an excellent nonlinear analysis method and spectral analysis method that is widely used in the field of geophysics [20], has also been applied to investigate the dynamic variation in vertical ozone. Compared with traditional

spectral analysis (such as Fourier analysis), the wavelet analysis method can find the variations of power with the time series and the local correlations and relative phases with other series. Furthermore, the wavelet analysis method can also provide the advance information for multiple regressions and the forecast of time series by using artificial intelligence [21]. Previous studies have employed the wavelet analysis method to study the variations in local or larger-area ozone concentrations and their coupling relationship with various climatic factors, including solar activity, atmospheric circulation, the ENSO, and QBO [22–27].

A long-term vertical ozone observational dataset was provided during 2001–2019 by ozonesonde measurements at the Beijing Nanjiao Meteorological Observatory (116.47° E, 39.81° N), which is located in the North China Plain, one of the most ozone-polluted regions in China [28,29]. This ozonesonde dataset is also a unique, available, in situ ozone measurement dataset that reveals the long-term variations in tropospheric and stratospheric ozone on the North China Plain, particularly around the Beijing region [30]. Previous studies using ozonesonde measurements over Beijing primarily focused on the vertical characteristics of climatological ozone and its variation (e.g., [7,31–34]); however, the dominant modes of ozone column variability and the driving factors (such as the ENSO, QBO, and 11-year solar activity cycle) of local ozone variation have not been well discussed from the perspective of time series analysis. Based on the above considerations, we first apply wavelet analysis to ozonesonde measurements in Beijing during 2001–2019 to explore the dominant modes of ozone variability over Beijing, and preliminarily discuss the driving factors (including the ENSO, QBO, and 11-year solar activity cycle) of ozone variability. The data and methods used in this study are described in Section 2. The main results of this study are presented in Section 3, and a conclusion is summarized in Section 4.

2. Data and Methods

2.1. Ozonesonde Measurements and Ozone Columns

The ozonesonde was routinely launched once a week during 2001–2019 to provide the ozone concentration from the ground to a height of ~35 km at the Nanjiao Meteorological Observatory in Beijing. The release time was ~14:00 China Standard Time when the maximum surface ozone concentration and highest mixed layer occurred. The average deviation of the ozone partial pressure originally measured by our ozonesonde and the ENSCI-Z ozonesonde [35,36] was <0.3 mPa, and the relative difference in the total ozone column from our ozonesonde and the ground-based Brewer spectrophotometer was 6% [30]. The monthly mean time series of TOT (Figure 1a), stratospheric column ozone (SCO) (Figure 1c), and tropospheric column ozone (TCO) (Figure 1e) during 2001–2019 over Beijing were calculated from ozonesonde measurements and Microwave Limb Sounder (MLS) ozone climatology. The TOT was calculated by integrating the ozone partial pressure up to 10 hPa or balloon burst (whichever came first) and then using MLS ozone climatology to estimate the amount of ozone above [37]; the TCO was calculated by integrating the ozone partial pressure from the ground to the tropopause derived from the ozonesonde measurements; and the SCO was the TOT minus the TCO. According to the World Meteorological Organization [38], the tropopause was defined as the lowest level where the temperature lapse rate fell below 2 K km^{-1} and where the average temperature lapse rate between this level and all the higher levels within 2 km remained below this value (in Figure 1e). The time series of TOT, TCO, and SCO were detrended and normalized before conducting the wavelet analysis in order to prevent the distortion of the spectrum and correlation function and to obtain the standardized wavelet power spectrum [20,39].

2.2. Climatic Indices

The Multivariate ENSO index (MEI.v2) is the time series of the leading combined Empirical Orthogonal Function (EOF) of five different variables (sea level pressure, sea surface temperature, zonal and meridional components of the surface wind, and outgoing longwave radiation) over the tropical Pacific basin (30° S–30° N and 100° E–70° W). The

MEI can provide a more complete and flexible description of the ENSO phenomenon than can single-variable ENSO indices such as the SOI or Niño 3.4 SST. Negative values of the MEI ($\text{MEI} < -0.5$) over five consecutive overlapping three-month periods represent the cold ENSO phase (La Niña), while positive MEI values represent the warm ENSO phase (El Niño) [40,41]. The cycle of the ENSO event is 2–7 years, and the ENSO event generally lasts a few months (usually >3 months) to a year. The QBO index is derived from the zonal mean wind at 30 hPa over the equator, and a westerly (easterly) phase winter is considered to occur if the anomaly of the QBO index is positive (negative) [42]. The 10.7 cm solar radio flux (F10.7 index), as an important parameter characterizing the level of solar activity, has a good correspondence with the number of sunspots, and its value usually exceeds 200 SFU ($1 \text{ SFU} = 10^{-22} \text{ m}^{-2} \text{ Hz}^{-1}$) during the peak of sunspot activity [43]. The F10.7 index has been used in previous studies to investigate the relationship between ozone variation and solar activity [23,44]. The above climatic indices can be obtained from the website <https://www.cpc.ncep.noaa.gov/> (accessed on 4 October 2023).

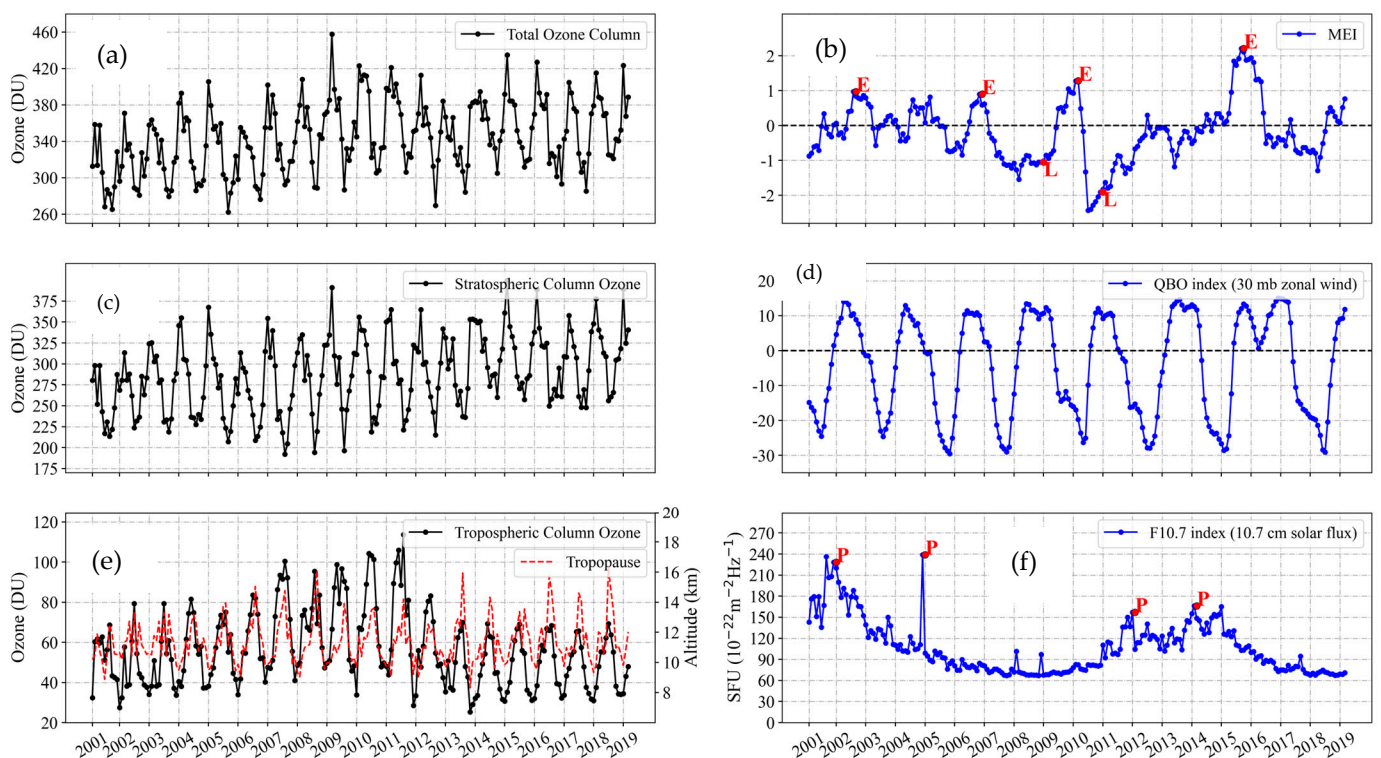


Figure 1. Time series of monthly total column ozone (TOT) (a), stratospheric column ozone (SCO) (c), and tropospheric column ozone (TCO) (e), the red dashed line in (e) is the monthly tropopause. (b,d,f) are time series of monthly MEI, QBO index, and F10.7 index, respectively. Some extraordinary time points mentioned in the text are marked by letters (E: El Niño events; L: La Niña events; P: peak sunspot activities) in (b,f).

2.3. Methods

The wavelet analysis methods used in this paper mainly include the continuous wavelet transform (CWT) and cross wavelet transform (XWT). CWT translates the time series into a time–frequency space to determine the principal patterns of time series variability and their temporal characteristics, whereas XWT unveils the relationship between two time series by analyzing their common power and relative phases in the time–frequency space [45]. CWT is similar to short-time Fourier transform and can be used to analyze time series containing nonstationary power at many different frequencies [46]. The wavelet

function $\psi_0(\eta)$ used in CWT is a function with a mean of zero, which is chosen as the Morlet wavelet function and consists of Gauss modulated plane waves in this study:

$$\psi_0(\eta) = \pi^{-1/4} e^{i\omega_0\eta} e^{-\eta^2/2} \quad (2)$$

where ω_0 is the dimensionless frequency, whose value is usually 6 to satisfy the admissibility condition [47], and η is a dimensionless time variable. CWT of a discrete sequence $\{x_n\}$ is defined as the convolution of $\{x_n\}$ with a scaled and translated version of $\psi_0(\eta)$:

$$W_n^X(s) = \sqrt{\frac{\delta t}{s}} \sum_{n'=1}^N x_{n'} \psi_0 \left[(n' - n) \frac{\delta t}{s} \right] \quad (3)$$

where s is the wavelet scale and n is the localized time index, and by using these two parameters, we can construct a picture showing both the amplitude of any features versus the scale and how this amplitude varies with time. The complex argument of $W_n^X(s)$ can be interpreted as the local phase, and the wavelet power is defined as $|W_n^X(s)|^2$. Since CWT is not completely localized in time and has edge effects, the concept of the cone of influence (COI) is thus introduced, which denotes the region where the edge discontinuous wavelet power drops to e^{-2} of the edge value, and the parts outside the COI are not considered. The significance level of the wavelet power spectrum is determined by comparison with the given background power spectrum P_k (usually the red noise standard spectrum) [20,45].

XWT of two time series $\{x_n\}$ and $\{y_n\}$ is defined as:

$$W_n^{XY}(s) = W_n^X(s) W_n^{Y*}(s) \quad (4)$$

where $*$ denotes complex conjugation, and the power of the cross wavelet is defined as $|W_n^{XY}(s)|$. The phase angle of W_n^{XY} can be interpreted as the local relative phase between x_n and y_n in the time–frequency space. For details on the significance test and the phase angle of XWT, please refer to Grinsted et al. [45] and Torrence et al. [20].

To better validate and analyze the power spectra of two time series after performing XWT, the sliding correlation coefficients (SCC) were introduced for auxiliary analysis. In Section 3.2, the SCC between the ENSO index and ozone columns was calculated using the ozone columns and MEI filtered through the 8th-order Butterworth high-pass filter, with a cutoff frequency of 1 year since the common high-power regions of XWT are concentrated near the annual cycle. The sliding window was set to 13, and each value represented the Pearson correlation coefficient for a period of 6 months before and after a time point. In the following sections, the calculation method for the SCC between the ozone column time series and the QBO or F10.7 indices was similar.

3. Results

3.1. CWT of Ozone Columns

The power spectra of the ozone columns after conducting CWT are shown in Figure 2. The high-power regions of the TOT, SCO, and TCO over Beijing that pass the significance test are concentrated near the annual cycle, indicating that these three ozone columns mainly obey the annual cycle variability pattern. Specifically, the TOT and SCO variations over Beijing are driven by the interannual circulation of BDC [21], which shows an interannual cycle pattern of high values in the cold season and low values in the warm season (see Figure 1a,c). The interannual variations in TCO were influenced by the seasonal variation in the thermodynamic first tropopause (as shown in Figure 1e). Furthermore, both the TOT and SCO exhibited strong high-frequency responses (~ 0.25 years) around 2007 and 2009, which may have been related to volcanic eruption events that could generate a significant impact on short-term ozone variations [27]. During these two periods, volcanic eruptions occurred at Tavorvur (4.23° S 152.20° E, October 2006) and Sarychev (48.09° N 153.20° E, June 2009), which could have resulted in an increase in sulfate aerosols that accelerated the heterogeneous chemistry and reduced the amount of ozone in the stratosphere. Given that

volcanic eruptions typically have strong geographic limitations [16], the influence on local ozone concentrations over Beijing may have been limited, and therefore, volcanic activity may not have been well detected in other years. As shown in Figure 2e, compared with the TOT and SCO, the variations in the TCO were more susceptible to high-frequency influencing factors, such as near-surface intense photochemical processes, stratospheric intrusion, biomass burning, and pollutant transport. The responses of the TCO to high-frequency influencing factors mainly occurred during the spring and summer periods in 2002, 2003, 2009, 2010, and 2012, which coincided with frequent pollutant transport from wildfire events in the vicinity of Beijing [34]. Since the narrowest part of the COI was only ~6 years in the time scale, it was difficult to reveal the relationship between the ozone column variations and lower-frequency events by using the wavelet power spectra to individual time series. From the global wavelet power spectra (in Figure 2), it appeared that the ozone columns in all three altitude ranges may have exhibited lower-frequency responses. For example, the TOT showed a high-power peak at a lower frequency of ~12 years, but these power values were not statistically significant. As discussed in the subsequent section, the analysis combining XWT and SCC will provide a better understanding of the relationship between ozone columns and lower-frequency events (climate events such as ENSO, QBO and the 11-year solar cycle) over Beijing.

3.2. XWT of Ozone Columns and Climatic Index

Figure 3 shows the XWT and SCC between the ozone columns and the ENSO index (MEI) over Beijing. From the regions that passed the significance test of the XWT power spectra, it was observed that the phase angle of the TCO consistently lagged behind that of the SCO by approximately $120^\circ \pm 15^\circ$, which corresponded to 1/3 of a cycle. The phase angle of the TOT was more similar to that of SCO because the variation in TOT was primarily determined by SCO. The TCO in the discussion above, calculated from the surface upward to the thermodynamic first tropopause, was mainly affected by variations in the tropopause. Although the ozone concentration always exhibits a high value in the troposphere during the warm season and in the stratosphere during the cold season [7], the phase lag is not exactly 1/2 of an annual cycle. Hence, the phase differences were reasonable among the ozone columns in the three altitude ranges in the XWT (the same was true between ozone columns and QBO and F10.7 indices). Detailed inspection of the XWT showed that the three ozone columns and MEI had a common high-power component in the annual cycle for the periods of 2002–2005, 2006–2007, 2009–2012, and 2014–2016. Combined with the corresponding SCC (Figure 3d–f), it was found that the XWT agreed well with the SCC, as shown around 2011, when the XWT between the TOT and MEI showed a clear in-phase variation and their SCCs also showed a significant positive correlation. Within the time periods above, both El Niño (warm-phase) and La Niña (cold-phase) events occurred. Taking the TOT and SCO as examples, for different warm-phase events occurring in different time periods, such as around the autumns of 2003, 2007, and 2016, the phase angle within the regions passing the significance test was $240^\circ \pm 30^\circ$ (stipulating that 0° for the rightward direction of the arrow and the phase angle increases clockwise). This indicated that warm-phase events always led the TOT and SCO variations by 1/4–1/2 of an annual cycle (approximately 3–6 months). Combined with Figure 1a,b, it could also be seen that the ENSO warm-phase peaks occurred around the end of the year and were approximately 3–6 months ahead of the TOT and SCO of the cold season peaks that passed the significance test. In general, similar to the results in other mid-latitude regions, the TOT and SCO in Beijing were also affected by ENSO warm-phase events and exhibited a hysteresis-positive anomaly response [15], and the hysteresis effect in this process could be explained by the ENSO delayed oscillator theory [48]. Moreover, the XWT and SCC between the ozone columns (TOT and SCO) and the MEI in Beijing showed obvious in-phase variations and significant positive correlations on the annual cycle during the strong cold–warm phase transition period in 2009–2012, which may have been related to the anomalous BDC and Eliassen–Palm flux dispersion [49].

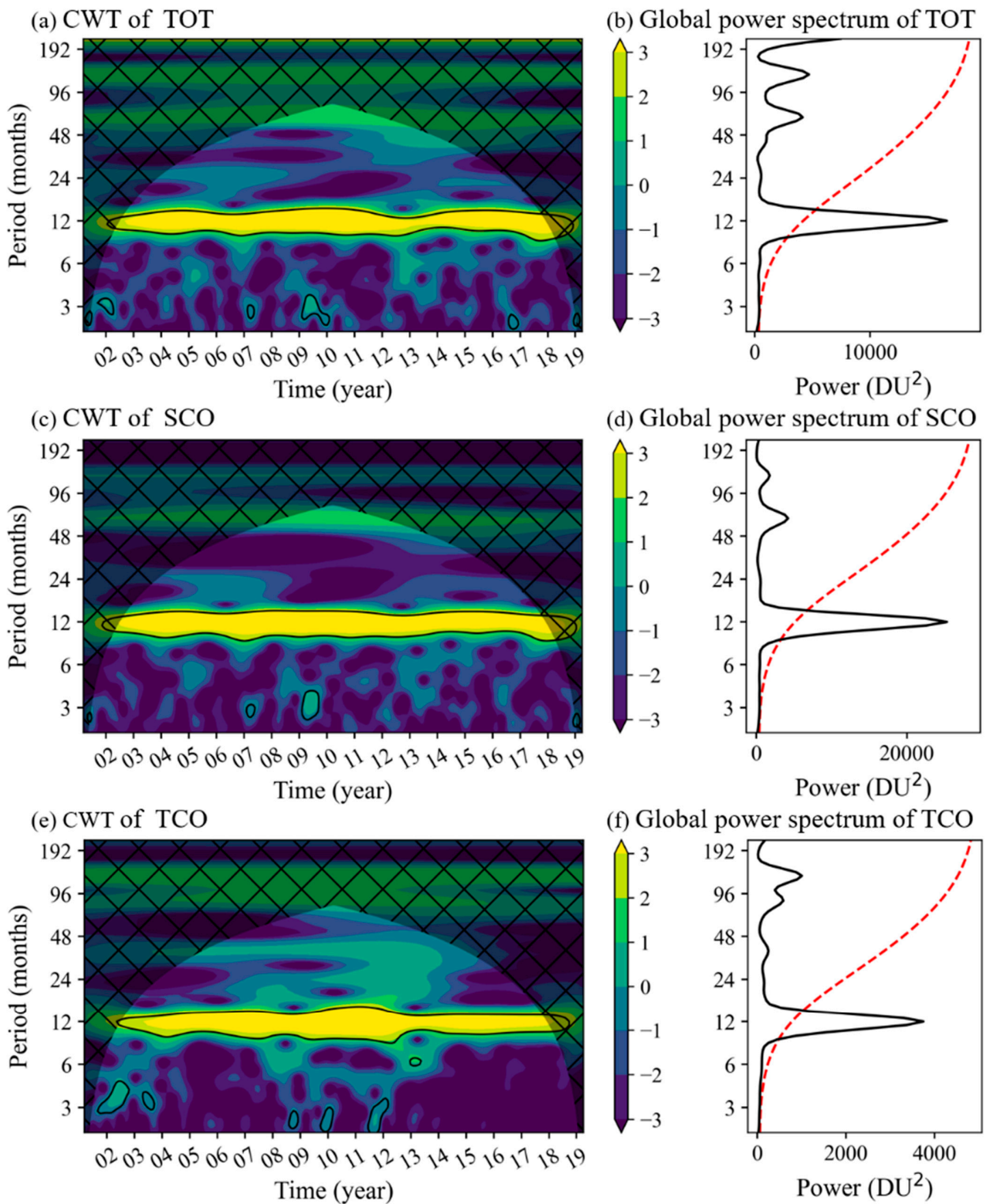


Figure 2. The background colors denote the CWT power spectra of TOT (a), SCO (c), and TCO (e); the cone of influence (COI) is shown as a lighter shade, and a thick contour designates the 5% significance level against red noise. (b,d,f) are the global wavelet power spectra of TOT, SCO, and TCO, respectively, in which the black line is the frequency distribution of power, and the red dotted line shows the 5% significance level.

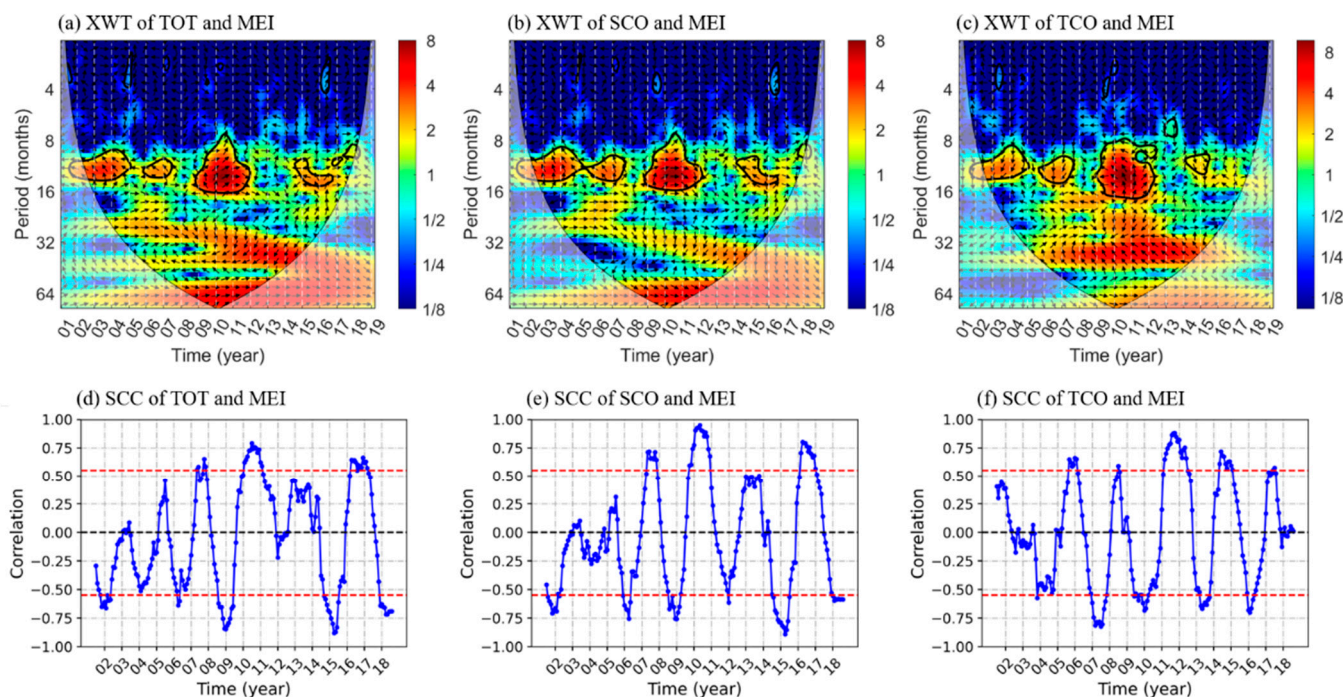


Figure 3. The background colors denote the XWT power spectra of MEI and TOT (a), SCO (b), and TCO (c), respectively; the COI is shown as a lighter shade, and thick contour designates the 5% significance level against red noise. The arrow indicates the relative phase difference (right: in-phase; left: anti-phase; down: X leading Y by 90 degrees; up: Y leading X by 90 degrees, X is the three ozone column time series, and Y is the climatic index in this study). The SCC (blue line) of MEI and TOT (d), SCO (e), and TCO (f) and the 5% significance level (red dotted line).

The XWT and SCC of the ozone columns over Beijing and the QBO index are shown in Figure 4, in which the XWT shows a continuous common high-power region on the annual cycle and a small portion of the common high-power region passing the significance test around the ~2-year cycle. The SCC (calculated using the time series of annual cycle components of the QBO and the monthly mean ozone columns) exhibited a significantly positive correlation over most of the time period, with a maximum SCC of 0.95 (0.90) between the TOT (SCO) and QBO. However, during the 2010–2012 period, the phase angle between the TOT (SCO) and QBO index was $270^\circ \pm 30^\circ$, in which the TOT (SCO) lagged behind the QBO changes; the phase angle between the TOT (SCO) and QBO index was $180^\circ \pm 30^\circ$ during the 2015–2017 period when the SCC showed a significant inverse correlation. Figure 1d further reveals that the abnormal fluctuation in the QBO index during the above two periods (2010–2012 and 2015–2017) led to the time-lagged variation in the correlation between the QBO index and ozone columns. In addition, compared with the TOT and SCO, the XWT of the TCO and QBO index (Figure 4c) showed a $\sim 90^\circ$ phase difference in the annual cycle since the response of the TCO to the QBO indicated the response of the tropopause to the QBO. The stratospheric mean meridional circulation (e.g., BDC, Hadley circulation) induced by the QBO in the tropics and mid-latitudes can cause anomalies in tropopause temperature and tropopause height [50]. According to Ribera et al. [51], the QBO signal variability in the mid-latitudes of the Northern Hemisphere led tropopause variability by approximately 1/4 of the annual cycle, which was similar to the results presented in this study. Overall, the ozone columns and QBO index over Beijing showed obvious correlations on an interannual cycle scale (i.e., seasonal correlation), with the TOT and SCO time series mostly positively correlated with the QBO index, and the TCO lagging behind the QBO by approximately 3 months in the seasonal correlation due to the influence of the thermodynamic tropopause. The reason for this phenomenon is the strong seasonality of the meridional circulation anomalies induced by the QBO. This process is

weaker during the summer in mid-latitude regions but stronger during the winter. The anomalous circulation modulating the QBO signal is the main cause of the anomalous ozone variations at mid-latitudes and in Beijing [52].

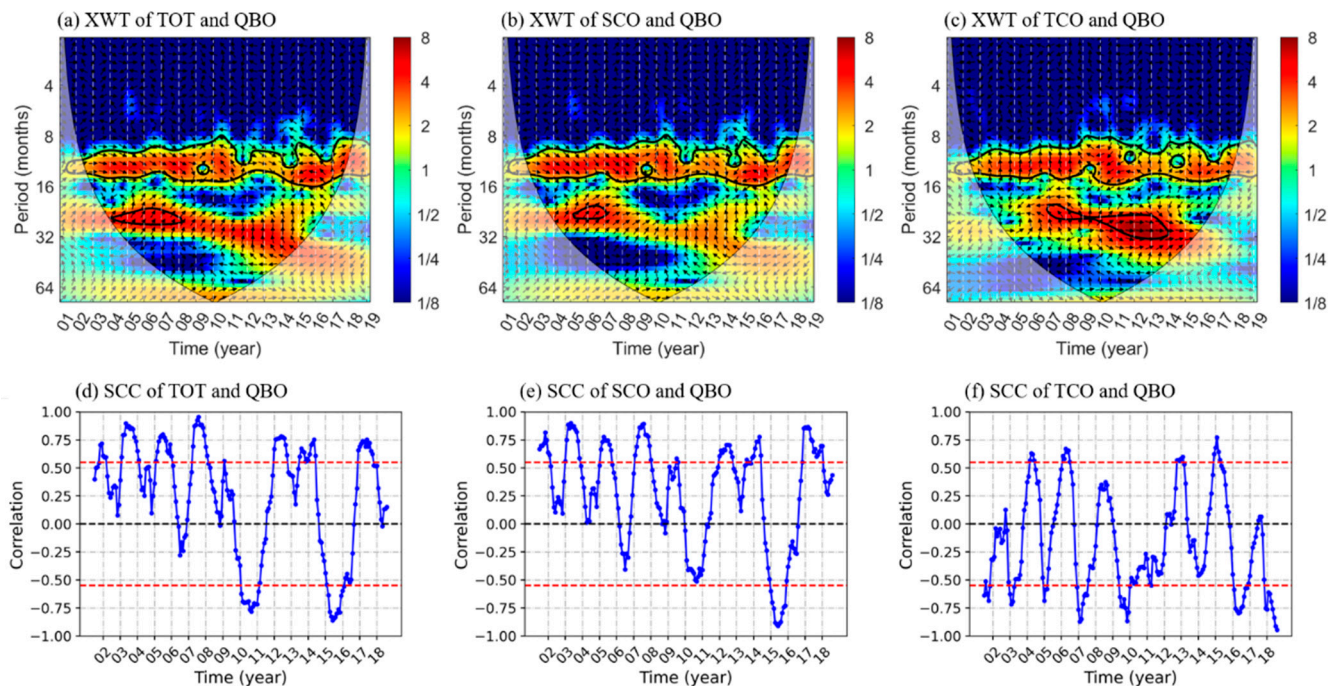


Figure 4. The background colors denote the XWT power spectra of the QBO index and TOT (a), SCO (b), and TCO (c); the COI is shown as a lighter shade, and the thick contour designates the 5% significance level against red noise. The arrow indicates the relative phase difference. The SCC (blue line) of QBO index and TOT (d), SCO (e), and TCO (f) and 5% significance level (red dotted line).

Finally, the relationship between the ozone columns and the solar activity index (F10.7) over three altitude ranges in Beijing was investigated. Since ~20 years of ozonesonde data in Beijing were available to cover only ~1.9 11-year solar cycles, the preliminary results discussed here have yet to be verified by accumulating longer time series of observational data. In Figure 1f, for the about two 11-year solar activity cycles throughout the study period, the peak of the first cycle was higher than that of the second cycle. Furthermore, the XWT of ozone columns and F10.7 (in Figure 5a–c) exhibited a high-frequency response only within a few periods, and no significant correlation was revealed by the SCC between the ozone columns and F10.7 (Figure 5d–f) over Beijing. The peaks of sunspot activity anomalies mainly occurred in 2002, 2005, 2012, and 2014 (Figure 1f). The periods of peak sunspot activities corresponded to the maximum positive anomalous response of the total ozone [53,54], during which the tropical or global ozone variations can be influenced by changes in solar UV spectral irradiance and changes in the flux of precipitation high-energy particles [23]. In summary, the total ozone has a certain lag response to the peak solar activity, which corresponds to the increase in total ozone; however, the correlation between the ozone columns over Beijing and the F10.7 index was not obvious except for a small part of the high-frequency response. This inapparent correlation might be explained as follows: (1) the ozone column time series in this study is relatively short, containing ~1.9 11-year solar activity cycles, which may make it difficult to comprehensively reveal the impact of solar activity; (2) the change caused by the solar activity was suggested only to be ~2% of the total ozone amount with a maximum change occurring at 2–3 hPa in the upper stratosphere [53,55]; and (3) the ozone columns over Beijing exhibit strong seasonal variations, which may mask the response of the ozone column to the solar cycle activity to some extent.

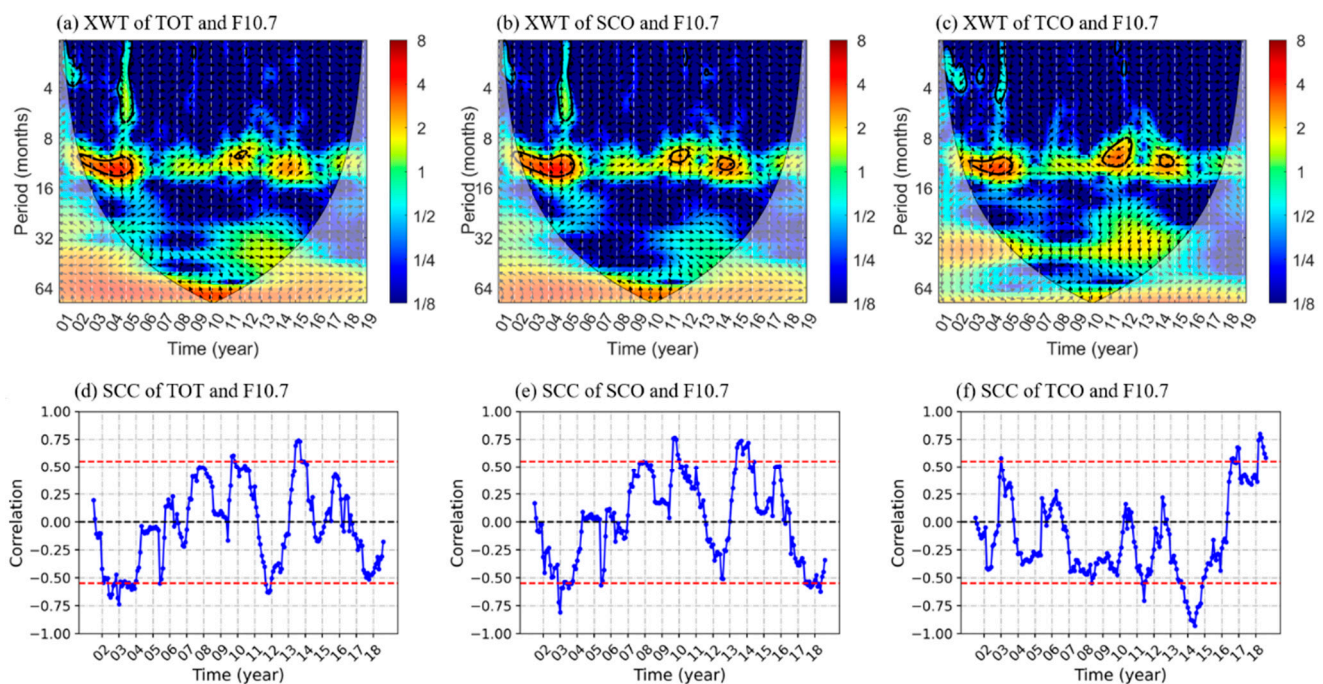


Figure 5. The background colors denote the XWT power spectra of the F10.7 index and TOT (a), SCO (b), and TCO (c); the COI is shown as a lighter shade, and a thick contour designates the 5% significance level against red noise. The arrow indicates the relative phase difference. The SCC (blue line) of the F10.7 index, TOT (d), SCO (e), and TCO (f), and the 5% significance level (red dotted line).

4. Conclusions and Discussions

By using ~20 years of ozonesonde measurements over Beijing to construct monthly time series of ozone columns in three altitude ranges (TOT, SCO, and TCO), this study applied the wavelet analysis method and sliding correlation coefficients algorithm to investigate the dominant modes of ozone column variability and its relationship with the climatic indices of ENSO, QBO, and solar activity cycle. The main conclusions are summarized as follows.

The continuous wavelet transform analysis revealed that ozone columns in the three altitude ranges showed strong interannual variability patterns, among which the high-frequency responses of TOT and SCO in 2007 and 2009 may have been related to the eruptive activities of Tavorvur and Sarychev. Compared to the TOT and SCO, the TCO was more susceptible to high-frequency influencing factors that coincided with pollutant transport from wildfire events around the Beijing ozonesonde site reported by [34]. The cross wavelet transform and slip correlation coefficient analyses showed that the relationships between the ozone columns and the ENSO and QBO over Beijing were consistent with those in other mid-latitude regions. During the ENSO warm phase periods that passed the significance test in 2003, 2007, and 2016, the TOT and SCO revealed positive anomalous responses to the ENSO warm phase events, and the ENSO warm phase peaks were approximately 3–6 months ahead of the winter peaks of the TOT and SCO. During the transition period of the strong cold-warm phase from 2009 to 2012, there was a significant positive correlation in the annual cycle between the variations in ozone columns and the ENSO index. The QBO-driven meridional circulation process was characterized by strong interannual variability, which led to a significant interannual positive correlation between the QBO index and the ozone columns (TOT and SCO) over Beijing, except for two anomalous fluctuations in 2010–2012 and 2015–2017. The TCO lagged behind the QBO variations in the correlation by approximately 3 months due to the influence of the thermodynamic tropopause. In general, no obvious correlation was shown between the solar activity index (F10.7) and the variations in the ozone columns over Beijing, which may have been due to the reasons such

as the relatively short time series analyzed (~1.9 11-year solar activity cycles), the relatively small changes of ozone columns caused by solar activity, and strong seasonal variations of the ozone columns in this study. The accumulation of longer time series of observational data may help comprehensively recognize the response of the ozone column to the solar cycle activity over Beijing region.

In this study, we utilized the wavelet analysis method to study the driving factors of the abnormal ozone concentration over Beijing and the time period of their occurrence. However, the driving mechanisms of the climatic factors on ozone variation are complex, especially for localized ozone variability, and there are also interactions between different climatic factors. The preliminary results presented in this study were derived based on ~20 years of ozonesonde measurements and climatic indices, and the mechanism between a climatic factor (especially the solar cycle activity) and ozone variation may still need to be further verified by accumulating longer time series of observations and other auxiliary data (such as the reanalysis data and satellite data). Furthermore, we can combine the observational data and chemical model such as WRF-CHEM or WRF-CMAQ [56–60], which can set up the sensitivity test for more in-depth qualitative or quantitative analysis of a chemical or physical process that affects ozone variability. The adoption of such a chemical model can facilitate a better understanding of the variations in ozone at different altitudes over Beijing and their driving mechanisms.

Author Contributions: Y.Z.: conceptualization, methodology, writing—original draft. J.Z.: conceptualization, methodology, writing—original draft, writing—review and editing. Y.L.: conceptualization, methodology, writing—review and editing. S.L.: conceptualization, methodology, writing—review and editing. H.C.: conceptualization, writing—review and editing. All authors have read and agreed to the published version of the manuscript.

Funding: This research was funded by the National Natural Science Foundation of China (Grant Nos. 42293321 and 41875183).

Data Availability Statement: The climatic index in this study can be obtained from the website <https://www.cpc.ncep.noaa.gov/> (accessed on 4 October 2023).

Acknowledgments: The authors thank the Beijing Nanjiao Meteorological Observatory for assisting in ozonesonde launches. We extend thanks to Yuejian Xuan and Xiaowei Wan for developing and launching the ozonesonde in this study.

Conflicts of Interest: The authors declare no conflict of interest.

References

1. Shindell, D.; Rind, D.; Balachandran, N.; Lean, J.; Lonergan, P. Solar cycle variability, ozone, and climate. *Science* **1999**, *284*, 305–308. [[CrossRef](#)] [[PubMed](#)]
2. Lefohn, A.S.; Malley, C.S.; Smith, L.; Wells, B.; Hazucha, M.; Simon, H.; Naik, V.; Mills, G.; Schultz, M.G.; Paoletti, E.; et al. Tropospheric ozone assessment report: Global ozone metrics for climate change, human health, and crop/ecosystem research. *Elem. Sci. Anthr.* **2018**, *6*, 27. [[CrossRef](#)] [[PubMed](#)]
3. Ball, W.T.; Alsing, J.; Staehelin, J.; Davis, S.M.; Froidevaux, L.; Peter, T. Stratospheric ozone trends for 1985–2018: Sensitivity to recent large variability. *Atmos. Chem. Phys.* **2019**, *19*, 12731–12748. [[CrossRef](#)]
4. Randel, W.J.; Stolarski, R.S.; Cunnold, D.M.; Logan, J.A.; Newchurch, M.; Zawodny, J.M. Trends in the vertical distribution of ozone. *Science* **1999**, *285*, 1689–1692. [[CrossRef](#)] [[PubMed](#)]
5. Grewe, V. The origin of ozone. *Atmos. Chem. Phys.* **2006**, *6*, 1495–1511. [[CrossRef](#)]
6. Zhang, J.; Li, D.; Bian, J.; Bai, Z. Deep stratospheric intrusion and Russian wildfire induce enhanced tropospheric ozone pollution over the northern Tibetan Plateau. *Atmos. Res.* **2021**, *259*, 105662. [[CrossRef](#)]
7. Zhang, J.; Li, D.; Bian, J.; Xuan, Y.; Chen, H.; Bai, Z.; Wan, X.; Zheng, X.; Xia, X.; Lü, D. Long-term ozone variability in the vertical structure and integrated column over the North China Plain: Results based on ozonesonde and Dobson measurements during 2001–2019. *Environ. Res. Lett.* **2021**, *16*, 074053. [[CrossRef](#)]
8. Krzyściński, J.W. On the interannual oscillations in the northern temperate total ozone. *J. Geophys. Res. Atmos.* **1994**, *99*, 14527–14534. [[CrossRef](#)]
9. Chehade, W.; Weber, M.; Burrows, J. Total ozone trends and variability during 1979–2012 from merged data sets of various satellites. *Atmos. Chem. Phys.* **2014**, *14*, 7059–7074. [[CrossRef](#)]

10. Baldwin, M.P.; Gray, L.J.; Dunkerton, T.J.; Hamilton, K.; Haynes, P.H.; Randel, W.J.; Holton, J.R.; Alexander, M.J.; Hirota, I.; Horinouchi, T.; et al. The quasi-biennial oscillation. *Rev. Geophys.* **2001**, *39*, 179–229. [[CrossRef](#)]
11. Zhang, J.; Zhang, C.; Zhang, K.; Xu, M.; Duan, J.; Chipperfield, M.P.; Feng, W.; Zhao, S.; Xie, F. The role of chemical processes in the quasi-biennial oscillation (QBO) signal in stratospheric ozone. *Atmos. Environ.* **2021**, *244*, 117906. [[CrossRef](#)]
12. Holton, J.R. Influence of the annual cycle in meridional transport on the quasi-biennial oscillation in total ozone. *J. Atmos. Sci.* **1989**, *46*, 1434–1439. [[CrossRef](#)]
13. Randel, W.J.; Garcia, R.R.; Calvo, N.; Marsh, D. ENSO influence on zonal mean temperature and ozone in the tropical lower stratosphere. *Geophys. Res. Lett.* **2009**, *36*, 15. [[CrossRef](#)]
14. Oman, L.D.; Douglass, A.R.; Ziemke, J.R.; Rodriguez, J.M.; Waugh, D.W.; Nielsen, J.E. The ozone response to ENSO in Aura satellite measurements and a chemistry-climate simulation. *J. Geophys. Res. Atmos.* **2013**, *118*, 965–976. [[CrossRef](#)]
15. Cagnazzo, C.; Manzini, E.; Calvo, N.; Douglass, A.R.; Akiyoshi, H.; Bekki, S.; Chipperfield, M.; Dameris, M.; Deushi, M.; Fischer, A.; et al. Northern winter stratospheric temperature and ozone responses to ENSO inferred from an ensemble of Chemistry Climate Models. *Atmos. Chem. Phys.* **2009**, *9*, 8935–8948. [[CrossRef](#)]
16. Lee, H.; Smith, A. Simulation of the combined effects of solar cycle, quasi-biennial oscillation, and volcanic forcing on stratospheric ozone changes in recent decades. *J. Geophys. Res. Atmos.* **2003**, *108*, D2. [[CrossRef](#)]
17. Li, Y.; Chipperfield, M.P.; Feng, W.; Dhomse, S.S.; Pope, R.J.; Li, F.; Guo, D. Analysis and attribution of total column ozone changes over the Tibetan Plateau during 1979–2017. *Atmos. Chem. Phys.* **2020**, *20*, 8627–8639. [[CrossRef](#)]
18. Xie, F.; Li, J.; Tian, W.; Zhang, J.; Sun, C. The relative impacts of El Niño Modoki, canonical El Niño, and QBO on tropical ozone changes since the 1980s. *Environ. Res. Lett.* **2014**, *9*, 064020. [[CrossRef](#)]
19. Zhou, L.; Zou, H.; Ma, S.; Li, P. The Tibetan ozone low and its long-term variation during 1979–2010. *Acta Meteorol. Sin.* **2013**, *27*, 75–86. [[CrossRef](#)]
20. Torrence, C.; Compo, G.P. A practical guide to wavelet analysis. *Bull. Am. Meteorol. Soc.* **1998**, *79*, 61–78. [[CrossRef](#)]
21. Werner, R. The latitudinal ozone variability study using wavelet analysis. *J. Atmos. Sol.-Terr. Phys.* **2008**, *70*, 261–267. [[CrossRef](#)]
22. Bencherif, H.; Tohir, A.M.; Mbatha, N.; Sivakumar, V.; du Preez, D.J.; Bègue, N.; Coetzee, G. Ozone Variability and Trend Estimates from 20-Years of Ground-Based and Satellite Observations at Irene Station, South Africa. *Atmosphere* **2020**, *11*, 1216. [[CrossRef](#)]
23. Echer, E. Multi-resolution analysis of global total ozone column during 1979–1992 Nimbus-7 TOMS period. *Ann. Geophys.* **2004**, *22*, 1487–1493. [[CrossRef](#)]
24. Fadnavis, S.; Beig, G. Spatiotemporal variation of the ozone QBO in MLS data by wavelet analysis. *Ann. Geophys.* **2008**, *26*, 3719–3730. [[CrossRef](#)]
25. Fadnavis, S.; Beig, G. Quasi-biennial oscillation in ozone and temperature over tropics. *J. Atmos. Sol.-Terr. Phys.* **2009**, *71*, 257–263. [[CrossRef](#)]
26. Okoro, E.C.; Yan, Y.-H.; Bisoi, S.K.; Zhang, Y. Response and periodic variation of total atmospheric ozone to solar activity over Mountain Waliguan. *Adv. Space Res.* **2021**, *68*, 2257–2271. [[CrossRef](#)]
27. Yang, J. Driving Force of Total Ozone in the Northern Midlatitudes: An Analysis based on Data from Two Stations. In Proceedings of the IGARSS 2019–2019 IEEE International Geoscience and Remote Sensing Symposium, Yokohama, Japan, 28 July–2 August 2019; pp. 7813–7816. [[CrossRef](#)]
28. Dufour, G.; Eremenko, M.; Beekmann, M.; Cuesta, J.; Foret, G.; Fortems-Cheiney, A.; Lachâtre, M.; Lin, W.; Liu, Y.; Xu, X.; et al. Lower tropospheric ozone over the North China Plain: Variability and trends revealed by IASI satellite observations for 2008–2016. *Atmos. Chem. Phys.* **2018**, *18*, 16439–16459. [[CrossRef](#)]
29. Dufour, G.; Hauglustaine, D.; Zhang, Y.; Eremenko, M.; Cohen, Y.; Gaudel, A.; Siour, G.; Lachatre, M.; Bense, A.; Bessagnet, B.; et al. Recent ozone trends in the Chinese free troposphere: Role of the local emission reductions and meteorology. *Atmos. Chem. Phys.* **2021**, *21*, 16001–16025. [[CrossRef](#)]
30. Zhang, J.; Xuan, Y.; Yan, X.; Liu, M.; Tian, H.; Xia, X.A.; Pang, L.; Zheng, X. Development and preliminary evaluation of a double-cell ozonesonde. *Adv. Atmos. Sci.* **2014**, *31*, 938–947. [[CrossRef](#)]
31. Zhang, Y.; Tao, M.; Zhang, J.; Liu, Y.; Chen, H.; Cai, Z.; Konopka, P. Long-term variations in ozone levels in the troposphere and lower stratosphere over Beijing: Observations and model simulations. *Atmos. Chem. Phys.* **2020**, *20*, 13343–13354. [[CrossRef](#)]
32. Tang, G.; Liu, Y.; Zhang, J.; Liu, B.; Li, Q.; Sun, J.; Wang, Y.; Xuan, Y.; Li, Y.; Pan, J.; et al. Bypassing the NO_x titration trap in ozone pollution control in Beijing. *Atmos. Res.* **2021**, *249*, 105333. [[CrossRef](#)]
33. Liao, Z.; Pan, Y.; Ma, P.; Jia, X.; Cheng, Z.; Wang, Q.; Dou, Y.; Zhao, X.; Zhang, J.; Quan, J. Meteorological and chemical controls on surface ozone diurnal variability in Beijing: A clustering-based perspective. *Atmos. Environ.* **2023**, *295*, 119566. [[CrossRef](#)]
34. Zeng, Y.; Zhang, J.; Li, D.; Liao, Z.; Bian, J.; Bai, Z.; Shi, H.; Xuan, Y.; Yao, Z.; Chen, H. Vertical distribution of tropospheric ozone and its sources of precursors over Beijing: Results from ~20 years of ozonesonde measurements based on clustering analysis. *Atmos. Res.* **2023**, *284*, 1066. [[CrossRef](#)]
35. Kerr, J.B.; Fast, H.; McElroy, C.; Oltmans, S.; Lathrop, J.; Kyro, E.; Paukkunen, A.; Claude, H.; Köhler, U.; Sreedharan, C.; et al. The 1991 WMO international ozonesonde intercomparison at Vanscoy, Canada. *Atmos.-Ocean* **1994**, *32*, 685–716. [[CrossRef](#)]
36. Florin, M.; Murariu, G.; Ionut, M.; Georgescu, L.P.; Topa, C.M. Preliminary results on atmospheric monitoring by means of a high-altitude balloon. *Ann. Univ. Dunarea Jos Galati Fascicle II Math. Phys. Theor. Mech.* **2011**, *34*.

37. McPeters, R.D.; Labow, G.J. Climatology 2011: An MLS and sonde derived ozone climatology for satellite retrieval algorithms. *J. Geophys. Res. Atmos.* **2012**, *117*, D10. [[CrossRef](#)]
38. WMO. Meteorology—A three-dimensional science. *WMO Bull.* **1957**, *6*, 134–138.
39. Andreas, E.L.; Treviño, G. Using Wavelets to Detect Trends. *J. Atmos. Ocean. Technol.* **1997**, *14*, 554–564. [[CrossRef](#)]
40. Baddoo, T.; Guan, Y.; Zhang, D.; Andam-Akorful, S. Rainfall Variability in the Huangfuchuang Watershed and Its Relationship with ENSO. *Water* **2015**, *7*, 3243–3262. [[CrossRef](#)]
41. Wolter, K.; Timlin, M.S. El Niño/Southern Oscillation behaviour since 1871 as diagnosed in an extended multivariate ENSO index (MEI.ext). *Int. J. Climatol.* **2011**, *31*, 1074–1087. [[CrossRef](#)]
42. Wang, L.; Wang, L.; Chen, W.; Huangfu, J. Modulation of winter precipitation associated with tropical cyclone of the western North Pacific by the stratospheric Quasi-Biennial oscillation. *Environ. Res. Lett.* **2021**, *16*, 054004. [[CrossRef](#)]
43. Tapping, K. The 10.7 cm solar radio flux (F10.7). *Space Weather* **2013**, *11*, 394–406. [[CrossRef](#)]
44. Londhe, A.; Bhosale, C.; Kulkarni, J.; Kumari, B.P.; Jadhav, D. Space-time variability of ozone over the Indian region for the period 1981–1998. *J. Geophys. Res. Atmos.* **2003**, *108*, D24. [[CrossRef](#)]
45. Grinsted, A.; Moore, J.C.; Jevrejeva, S. Application of the cross wavelet transform and wavelet coherence to geophysical time series. *Nonlinear Process. Geophys.* **2004**, *11*, 561–566. [[CrossRef](#)]
46. Daubechies, I. The wavelet transform, time-frequency localization and signal analysis. *IEEE Trans. Inf. Theory* **1990**, *36*, 961–1005. [[CrossRef](#)]
47. Foufoula-Georgiou, E.; Kumar, P.; Chui, C. *Wavelets in Geophysics*; Academic Press: Cambridge, MA, USA, 1994.
48. Ding, Y. Analysis of the process and mechanisms of genesis and development for 2014–2016 mega El Niño event. *Trans. Atmos. Sci.* **2016**, *39*, 722–734.
49. Lin, J.; Qian, T. Impacts of the ENSO Lifecycle on Stratospheric Ozone and Temperature. *Geophys. Res. Lett.* **2019**, *46*, 10646–10658. [[CrossRef](#)]
50. Ribera, P.; Peña-Ortiz, C.; Garcia-Herrera, R.; Gallego, D.; Gimeno, L.; Hernández, E. Detection of the secondary meridional circulation associated with the quasi-biennial oscillation. *J. Geophys. Res. Atmos.* **2004**, *109*, D18. [[CrossRef](#)]
51. Ribera, P.; Peña-Ortiz, C.; Añel, J.A.; Gimeno, L.; de la Torre, L.; Gallego, D. Quasi-biennial modulation of the Northern Hemisphere tropopause height and temperature. *J. Geophys. Res. Atmos.* **2008**, *113*, D7. [[CrossRef](#)]
52. Kinnersley, J.S.; Tung, K.K. Mechanisms for the extratropical QBO in circulation and ozone. *J. Atmos. Sci.* **1999**, *56*, 1942–1962. [[CrossRef](#)]
53. Chandra, S.; McPeters, R. The solar cycle variation of ozone in the stratosphere inferred from Nimbus 7 and NOAA 11 satellites. *J. Geophys. Res. Atmos.* **1994**, *99*, 20665–20671. [[CrossRef](#)]
54. Zerefos, C.; Tourpali, K.; Bojkov, B.; Balis, D.; Rognerund, B.; Isaksen, I. Solar activity-total column ozone relationships: Observations and model studies with heterogeneous chemistry. *J. Geophys. Res. Atmos.* **1997**, *102*, 1561–1569. [[CrossRef](#)]
55. Hauchecorne, A.; Bertaux, J.-L.; Lallement, R. Impact of solar activity on stratospheric ozone and NO₂ observed by GOMOS/ENVISAT. *Sol. Var. Planet. Clim.* **2007**, *23*, 393–402. [[CrossRef](#)]
56. Abdi-Oskouei, M.; Carmichael, G.; Christiansen, M.; Ferrada, G.; Roozitalab, B.; Sobhani, N.; Wade, K.; Czarnetzki, A.; Pierce, R.B.; Wagner, T.; et al. Sensitivity of meteorological skill to selection of WRF-Chem physical parameterizations and impact on ozone prediction during the Lake Michigan Ozone Study (LMOS). *J. Geophys. Res. Atmos.* **2020**, *125*, e2019JD031971. [[CrossRef](#)]
57. Sharma, A.; Ojha, N.; Pozzer, A.; Mar, K.A.; Beig, G.; Lelieveld, J.; Gunthe, S.S. WRF-Chem simulated surface ozone over south Asia during the pre-monsoon: Effects of emission inventories and chemical mechanisms. *Atmos. Chem. Phys.* **2017**, *17*, 14393–14413. [[CrossRef](#)]
58. Mar, K.A.; Ojha, N.; Pozzer, A.; Butler, T.M. Ozone air quality simulations with WRF-Chem (v3. 5.1) over Europe: Model evaluation and chemical mechanism comparison. *Geosci. Model Dev.* **2016**, *9*, 3699–3728. [[CrossRef](#)]
59. Wang, P.; Wang, P.; Chen, K.; Du, J.; Zhang, H. Ground-level ozone simulation using ensemble WRF/Chem predictions over the Southeast United States. *Chemosphere* **2022**, *287*, 132428. [[CrossRef](#)]
60. Mak, H.W.L. Improved Remote Sensing Algorithms and Data Assimilation Approaches in Solving Environmental Retrieval Problems. Ph.D. Thesis, Hong Kong University of Science and Technology, Hong Kong, China, 2019.

Disclaimer/Publisher’s Note: The statements, opinions and data contained in all publications are solely those of the individual author(s) and contributor(s) and not of MDPI and/or the editor(s). MDPI and/or the editor(s) disclaim responsibility for any injury to people or property resulting from any ideas, methods, instructions or products referred to in the content.